EVALUATION OF NONLINEAR EFFECTS IN THE 3-GeV RAPID CYCLING SYNCHROTRON OF J-PARC

H. Hotchi*, F. Noda, N. Tani, JAERI, Tokai, Ibaraki, JAPAN
J. Kishiro, S. Machida, A. Yu. Molodojentsev, KEK, Tsukuba, Ibaraki, JAPAN

Abstract

The 3-GeV *R*apid *C*ycling *S*ynchrotron (*RCS*) of J-PARC is designed to accelerate 8.3×10^{13} protons per pulse up to 3 GeV at a repetition rate of 25 Hz. In order to implement the painting injection which is effective to defuse the space-charge force and to gain an excellent collimation efficiency, the RCS has a large acceptance in comparison with ordinary rings, which leads to a large aspect ration of the magnets (inner diameter over magnet length). In such a case, intrinsic field nonlinearities play a significant role, and the nonlinear behavior of particles at large amplitude and large momentum deviation is a essential issue. In this paper, we discuss influences of the intrinsic field nonlinearity of the main dipole magnet and combined effects with the sextupole field utilized for the chromatic correction. In addition, a possible correction scheme for the induced betatron resonances is discussed.

INTRODUCTION

The RCS has a three-fold symmetric lattice over its circumference of 348.333 m [1]. Each super-period consists of two 3-DOFO arc modules and a 3-DOFO insertion. Each arc module has a missing-bend cell, where the horizontal dispersion has the maximum value. Three families of sextupole magnets are prepared at each missing-bend cell and utilized for the chromatic correction. The insertions are dispersion free. The injection and collimation systems occupy one of the three insertions; the injection system uses the first one and a half cells and the collimator system takes the rest. The extraction and RF systems are each allocated in the other two insertions.

The key issue in the design of the RCS is to control and localize the beam loss and decrease the uncontrolled beam loss. For this purpose, the transverse painting injection is designed to control the beam density and to suppress the space-charge effect. An adequate ratio between the physical and collimator apertures is another important factor to localize the beam loss. The painting emittance and collimator acceptance are each 216π and 324π mm mrad. For those values, the ring acceptance (486π mm mrad) 1.5 times larger than the collimator acceptance is secured for a possible momentum spread of $\pm1\%$ to keep a sufficient collimation efficiency ($\sim$99.7%).

In such synchrotrons with large aperture, it becomes important to consider intrinsic field nonlinearities, and the nonlinear motion of the beam particles, especially moving away from the axis of the elements, is a common issue.

* hotchi@linac.tokai.jaeri.go.jp

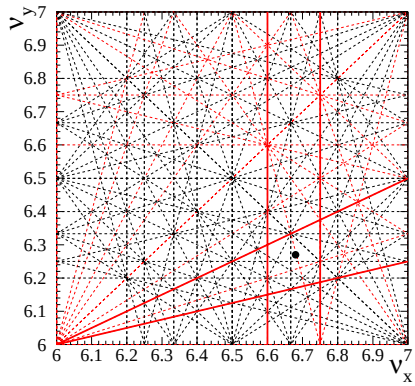

Figure 1: Tune diagram up to 5th-order resonances around the nominal operating point (6.68, 6.27) of the RCS. The solid lines show anxious nonlinear structure resonances lying near the nominal tune.

Nonlinear fields drive high-order transverse resonances. Fig. 1 shows a tune diagram up to 5th-order resonances around the nominal operating point (ν_x, ν_y)=(6.68, 6.27) of the RCS, where the ν_x and ν_y are the horizontal and vertical betatron tunes. In these resonances the solid lines correspond to anxious nonlinear structure resonances at the RCS. While the nominal operating point is chosen to avoid the structure resonances, the beam will cross some of them due to the space-charge incoherent tune shift which is expected to be 0.15$\sim$0.25. The stability and flexibility in the betatron tune space are required to keep alternate working points as well as to cover the possible incoherent tune shift. For this concern, we have first evaluated influences of the intrinsic field nonlinearity of the main dipole magnet and combined effects with the sextupole field utilized for the chromatic correction, and discussed a correction scheme for the induced transverse resonances.

MODELING OF THE MULTIPOLE FIELD IN THE MAIN DIPOLE MAGNET

The main parameters of the dipole magnet is listed in Fig. 2-(a). The field measurement for the dipole magnets have started very recently. Therefore, we have first investigated effects of nonlinear field components of the dipole magnet using the output of the TOSCA-3D corresponding to the injection energy of 181 MeV (it will be upgraded to 400 MeV after the operation starts). The calculated field has a midplane-symmetric distribution for the X-Z plane and is mirror-symmetric for the X-Y plane in the coordinate defined in Fig. 2-(a).

At first we estimated a beam path in the dipole magnet

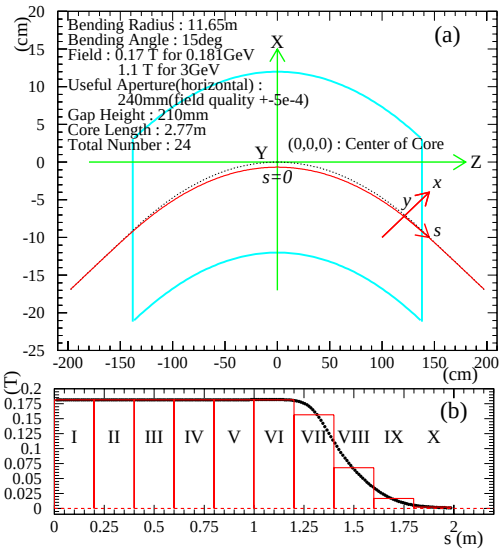

Figure 2: (a) Beam path in the dipole magnet. The dotted curve is the central orbit obtained for the uniform dipole field without any fringe field, while the solid one is that estimated by tracking with the TOSCA-3D field, which passes through ∼6.7 mm-inside of the center of the magnet in this geometric condition due to the fringe field. (b) Field distribution of B_y along the solid curve in (a).

as shown in Fig. 2-(a). In the figure, the dotted curve shows the ideal central orbit obtained for the uniform dipole field without any fringe field, while the solid one is the central orbit estimated by tracking with the TOSCA-3D field. The field distribution along the solid curve is shown in Fig. 2-(b). Due to the fringe field, the actual central orbit was estimated to pass through ∼6.7 mm-inside of the center of the magnet in this geometric condition. The multipole field components of the dipole magnet were evaluated along this estimated reference orbit.

Assuming x and $y \ll \rho$, the magnetic field can be expanded as

$$B_y + jB_x = \sum_{n=0} b_{n,0}(x+jy)^n - \frac{b''_{0,0}}{2}y^2 - \frac{b''_{1,0}}{2}(x+jy)y^2\cdots, \quad (1)$$

where the coordinate is defined in Fig. 2-(a), the ρ is the bending radius, $b_{n,0}=\frac{1}{n!}\frac{\partial^n B_y}{\partial x^n}$, and the prime is the derivative with respect to s. In the present analysis, the coefficients $b_{n,0}$, $b''_{0,0}$ and $b''_{1,0}$ were determined by fitting the B_y versus x distribution on the medium plane with a polynomial: we made sure the field distribution on the off-medium plane can be reproduced reasonably well using Eq. (1).

The fringe field with $b''_{0,0}$, $b''_{1,0}\neq 0$ has a sextupole-like and an octupole-like field component. However the effects of $b''_{0,0}$ and $b''_{1,0}$ tend to be canceled out due to the characteristic shape of the fringe field and the nonlinear motion of the beam particle can be effectively simulated simply by considering the pure multipole field components $b_{n,0}$. As shown in Fig. 2-(b), the field area was divided into 10 regions, and the multipole field components $K_n=\frac{n!}{B\rho}\int b_{n,0}ds$ were evaluated for each region as shown in Fig. 3, where the $B\rho$ is the magnetic rigidity. They were introduced as thin lens at the center of each region for our tracking simulations.

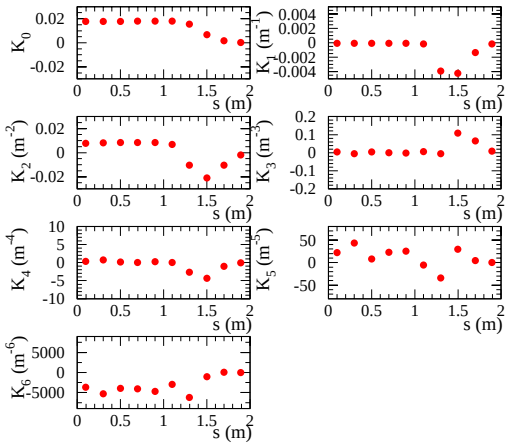

Figure 3: Multipole field strengths of the dipole magnet $K_n=\frac{1}{B\rho}\int\frac{\partial^n B_y}{\partial x^n}ds$, in which each data point corresponds to K_n evaluated for each segment shown in Fig. 2-(b).

TRACKING SIMULATION

We performed single-particle tracking simulations considering the calculated field distribution of the dipole magnet with two separated methods. The first is the tracking with the code called SAD [2], in which the multipole field components of the dipole magnet were introduced as thin lens as described in the last section. The second method is the 4th-order Runge-Kutta tracking directly with the TOSCA-3D field of the dipole magnet. Though the former method can execute a faster tracking, it has some ambiguity for the modeling. On the other hand, the latter one is more direct simulation, while it takes somewhat larger computation time and the Runge-Kutta integrator itself is not symplectic. Therefore we checked the validity of our simulations by comparing with each other; the two separated results were in good agreement with each other, and thus it is expected our simulations reasonably catch the nonlinear motion of the beam particle. The analysis results by the first method are explained in the following (the details of the analysis by the Runge-Kutta tracking are in [3]).

Induced Nonlinear Resonances

In the present simulation, the multipole field components of the dipole magnet were included up to 14-pole and the chromatic correction sextupole magnets were excited. The natural chromaticity of the RCS is ∼-8.5 for both horizontal and vertical, and three families of sextupole magnets (SDA, SDB, SFX) are prepared for the chromatic correction. The sextupole strengths were set at $\frac{B_y^{(2)}L}{B\rho}$= -0.317 (SDA), -0.300 (SDB) and 0.380 (SFX) m^{-2}, which were

optimized to make the chromaticity zero at the nominal operating point (6.68, 6.27). In this simulation, the synchrotron oscillation was included assuming the stationary bucket. The physical apertures were set for all the main magnets and for a beam particle with the initial condition of ϵ_x=ϵ_y, x=$(\epsilon_x/\gamma_x)^{1/2}$, y=$(\epsilon_y/\gamma_y)^{1/2}$, x'=y'=0 we looked for the maximum value of ϵ_x=ϵ_y for which the beam survived within the physical apertures up to 5000 turns, where the x, x' and y, y' are the betatron phase space coordinates, the ϵ is the emittance and γ=$(1+\alpha^2)/\beta$ of the betatron amplitude functions. Fig. 4-(a) and (b) show the maximum ϵ_x=ϵ_y for the beam survival as a function of ν_x and ν_y estimated for the on- and off-momentum beams of $\Delta p/p$=0 and 0.5%. As shown in these figures, several structure resonances are excited. The ν_x-2ν_y=-6 and 4ν_x=27 are excited mainly by the chromatic correction sextupole fields through first- and second-order perturbation expansion. The other higher-order resonances ν_x-4ν_y=-18 and 3ν_x+4ν_y=45 are induced by the high-order multipole field components of the dipole magnets. In these resonances, the 3rd-order ν_x-2ν_y=-6 resonance strongly limits the tunability of the RCS. Due to the space-charge tune depression (0.15∼0.25), we cannot set the operating point above the 3rd-order resonance. While the nominal tune is now set below the resonance, the location had better be slightly shifted toward the resonance to completely avoid the lower integer line ν_y=6 when the tune shift takes place. Thus, the correction of the ν_x-2ν_y=-6 is essential to keep the flexibility in the betatron tune space and to get more margin for the possible tune shift.

Correction of ν_x-2ν_y=-6

For this purpose, we will introduce two families of sextupole correctors at both ends of the dispersion-free insertion. The driving term of the 3rd-order ν_x-2ν_y=-6 resonance is expressed as

$$G_{1,-2,-6}e^{j\zeta} = -\frac{\sqrt{2}}{8\pi}\oint \frac{B_y^{(2)}}{B\rho}\sqrt{\beta_x\beta_y^2}\times \exp j\{\chi_x(s) - 2\chi_y(s) - (\nu_x - 2\nu_y + 6)\theta\}ds, \quad (2)$$

where the χ is the phase advance and the θ the orbiting angle. Its value originated from the chromatic correction sextupole field and the sextupole field component of the dipole magnet is estimated to be 0.923+j0.403 at the on-resonance point (6.56, 6.27), which can be canceled by the sextupole correctors with moderate field strengths of $\frac{B_y^{(2)}L}{B\rho}$∼0.1 m^{-2}. Fig. 4-(c) and (d) show the similar maps as Fig. 4-(a) and (b) after the 3rd-order resonance correction. As shown in the figures, the ν_x-2ν_y=-6 resonance significantly decays near the nominal operating point for both on- and off-momentum beam particles. This correction scheme supplies better tunability for the RCS.

SUMMARY AND FUTURE WORK

We performed single-particle tracking simulations considering the calculated field distribution of the main dipole magnet corresponding to the injection energy. The intrinsic nonlinear field components of the dipole magnet and the sextupole fields utilized for the chromatic correction excite some structure resonances, in which the 3rd-order ν_x-2ν_y=-6 resonance, which is excited mainly by the chromatic correction sextupole fields, chiefly limits the tunability of the RCS. The 3rd-order resonance can be corrected significantly by two families of sextupole correctors with moderate field strengths which will be introduced at both ends of the dispersion-free insertion.

There still remain various nonlinearities and imperfections which should be included in the simulation. For example, intrinsic nonlinear field components in the quadrupole magnets, leak fields from the injection and extraction beam line magnets, field and alignment errors, and so forth. We will first implement more realistic single-particle tracking simulations including the above effects and discuss further correction schemes if required. Then we will perform integrated multi-particle tracking simulations and optimize the operating pattern.

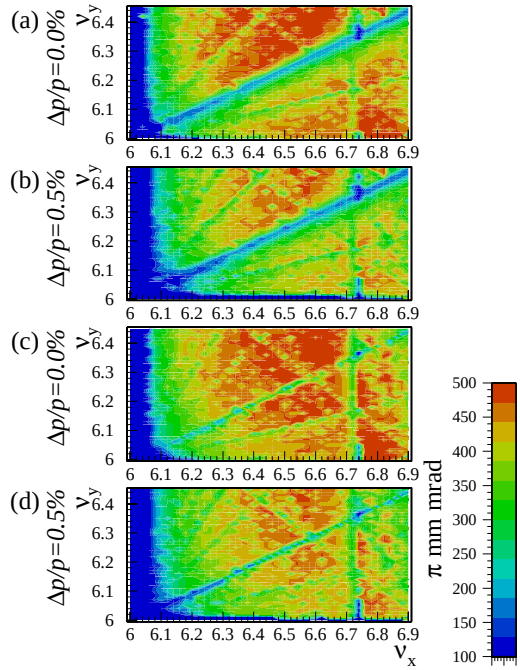

Figure 4: Maximum beam emittance ϵ_x=ϵ_y for the beam survival as a function of ν_x and ν_y estimated for the on- and off-momentum beams of $\Delta p/p$=0 and 0.5% around the nominal operating point (6.68, 6.27). The upper (a) and (b) show the maps before the correction for the ν_x-2ν_y=-6, while the lower (c) and (d) correspond to those after the correction.

REFERENCES

[1] "Accelerator Technical Design Report for High-Intensity Proton Accelerator Facility Project", JAERI-Tech 2003-044.

[2] http://acc-physics.kek.jp/SAD/sad.html.

[3] A. Yu. Molodojentsev *et al.*, "Dynamic Aperture and Resonance Correction for J-PARC RCS", Proc. of Particle Accelerator Conference, May 2005, Tennessee (to be published).